

DOUBLE NEUTRON STAR MERGERS: ARE LATE-TIME RADIO SIGNALS OVERESTIMATED?

SHAO-ZE LI^{1,5,6}, YUN-WEI YU², HE GAO^{3,4}, AND LIN LAN^{3,4}

Draft version February 29, 2024

ABSTRACT

The coalescence of binary neutron stars can yield the expulsion of a fast-moving, quasi-isotropic material, which may induce thermal radiation and give rise to kilonova emission. Moreover, the interaction between the ejected material and the surrounding environment generates an external shock, which can result in a long-lasting radio signal that persists for several decades following the merger. In contrast to supernova ejecta, the kilonova ejecta exhibits a relatively lesser mass and higher velocity, and its expansion may ultimately result in the ejecta density becoming so low that the medium particles can freely pass through the ejecta. It would thereby lead to a kind of incomplete sweeping on the interstellar medium. Employing a toy model, our investigation reveals that such incomplete sweeping may considerably diminish the late-time radio radiation power, irrespective of whether the binary neutron star merger results in the formation of a black hole or a neutron star. Our findings thus imply that the previously reported radio upper limits for certain short gamma-ray bursts (GRBs) may not necessarily place stringent constraints on the presence of a long-lived magnetar remnant in these short GRBs.

Subject headings: : Gamma-ray bursts (629); Gravitational waves (678); Neutron stars (1108); Interstellar medium (847)

1. INTRODUCTION

The first detection of a gravitational-wave (GW) signal from a merger of double neutron stars (NSs), GW170817, opens new era of multimessenger astronomy (Abbott et al. 2017a). The association of the GW, the short gamma-ray burst (GRB), and the kilonova signals confirms that at least some of the short GRBs come from mergers of NSs (Abbott et al. 2017b; Cowperthwaite et al. 2017; Nicholl et al. 2017; Pian et al. 2017; Smartt et al. 2017; Tanaka et al. 2017; Tanvir et al. 2017; Troja et al. 2017; Villar et al. 2017). It has been almost 6 yr since the detection of GW170817. However, it is still puzzling whether the merger remnant is a black hole (BH) or a massive NS (Sarin & Lasky 2021). In the literature, a millisecond magnetar is usually proposed as one candidate of the central engine of GRBs (Dai & Lu 1998a, 1998b; Zhang & Mészáros 2001; Metzger et al. 2011). Compared with the BH model, the magnetar model is helpful in understanding the observational features, such as the plateau and flares in the GRB afterglow emission (Vaughan et al. 2006; Falcone et al. 2007; Rowlinson et al. 2013; Lü et al. 2015; Gao et al. 2016). Mean-

while, the energy injection from the central magnetar powers the isotropic merger ejecta, resulting in the much brighter kilonova emission (mergernova; Yu et al. 2013, 2015, 2018; Metzger & Piro 2014; Gao et al. 2015, 2017; Metzger et al. 2017; Li et al. 2018; Ai et al. 2022; Sarin et al. 2022).

If the post-merger remnant is indeed a long-lived massive NS, rather than a BH, it would give stringent constraints on the equation of state of dense matter (Gao et al. 2016; Margalit & Metzger 2017; Shibata et al. 2017, 2019; Ai et al. 2018; Radice et al. 2018; Rezzolla et al. 2018; Ai et al. 2020). Metzger & Bower (2014) proposed that the isotropic radio afterglow of the merger ejecta can be used to test the merger remnant. Following the explosion of the ejecta, an external shock is formed and sweeps up the surrounding medium. Depending on specific parameters, the external shock could give a long-lasting radio signal several years or several tens of years after the merger (Nakar & Piran 2011). Due to the existence of the magnetar, the merger ejecta can be accelerated into relatively higher velocity, which results in much brighter radio emission (Gao et al. 2013). Based on this starting point, several works have tried to catch the radio signals from the GW170817 event and nearby short GRBs, but no signals were detected (Metzger & Bower 2014; Fong et al. 2016; Horesh et al. 2016; Klose et al. 2019; Schroeder et al. 2020; Bruni et al. 2021; Ricci et al. 2021). Their results give constraints on the central object, which seems to rule out a magnetar remnant with rotation energy beyond 10^{52} ergs. Nevertheless, Liu et al. (2020) point out that the magnetic field fraction factor ϵ_B is significant in calculating the radiation mechanism. Taking a relatively lower ϵ_B derived from GRB after-

¹ College of Physics Science and Technology, Hebei University, Baoding 071002, China; lishaoze@mails.cnu.edu.cn

² Institute of Astrophysics, Central China Normal University, Wuhan 430079, China; yuyw@mail.cnu.edu.cn

³ Institute for Frontier in Astronomy and Astrophysics, Beijing Normal University, Beijing 102206, China; gaohe@bnu.edu.cn

⁴ Department of Astronomy, Beijing Normal University, Beijing 100875, China

⁵ Hebei Key Laboratory of High-precision Computation and Application of Quantum Field Theory, Baoding, 071002, China

⁶ Hebei Research Center of the Basic Discipline for Computational Physics, Baoding, 071002, China

glows, they obtain the radio light curves using a more detailed model. The result shows that a magnetar remnant with rotation energy $\sim 10^{52}$ ergs is still allowed in broad parameter space.

In comparison to the supernova ejecta, the kilonova ejecta exhibits a significantly lesser mass and higher velocity. Moreover, Margalit & Piran (2020) proposed a relativistic jetted outflow in front of the ejecta, which would result in much earlier radio signals. No matter the ejecta or the jetted outflow, their density could eventually reach a low level as they expand to a certain extent. This would make the ejecta or outflow so rarefied that it would have hardly any significant interaction with the interstellar medium (ISM). Meanwhile, it may result in a kind of incomplete sweeping on the ISM. This effect has not previously been examined. To address the incomplete sweeping, we first discuss the free path of the ISM particles (ionized or neutral hydrogens) in Section 2. Subsequently, we demonstrate the limitations of the complete-sweeping assumption under typical conditions and construct an adapted toy model incorporating the incomplete-sweeping effect (Section 3). In Section 4, we reevaluate the dynamics of the ejecta and illustrate the discernible distinctions in the light curves of the late-time radio emission. Our concluding remarks and discussions are presented in Section 5.

2. THE FREE PATH

In many astrophysical explosion events, such as supernovae, GRBs, etc., the shock process usually plays a significant role in their dynamics as well as the emissions. As extensively discussed in the literature, a significant fraction of astrophysical shocks are collisionless, especially in low-density flows. Such shocks are characterized by plasma interactions instead of particle collisions. For a charged particle moving within a plasma, the free path is affected by the collective field, which operates on the scale of the plasma skin depth,

$$l_{\text{pl}} = \frac{c}{\omega_{\text{pe}}} \quad (1)$$

$$= 5.3 \times 10^5 n_e^{-1/2} \text{cm}, \quad (2)$$

where ω_{pe} is the electron plasma frequency. Such a free path is usually much less than the astrophysical flow scale. As a result, collisionless shocks can form during the interactions of plasma flows only if the relative velocity exceeds the local sound speed. But not all astrophysical flows are plasmas. If the flows consist of neutral molecules or atoms, there will be another scenario. For a neutral particle, the free path is dominated by elastic collisions:

$$l_{\text{co}} = (\sigma n_{\text{ej}})^{-1} \\ \approx 10^{15} n_e^{-1} \text{cm}, \quad (3)$$

where $\sigma \approx 10^{-15} \text{cm}^2$ is approximately the cross section of typical air molecules on the earth. Obviously, this free path is much longer than that in plasma. The precondition for the formation of a steady shock is $l \ll L$, which requires that the scale of flows must be large enough. A typical example of this scenario is the collisions between neutral molecular clouds.

In supernova-like events, it is usually assumed that the isotropic ejecta would interact with the ambient ISM

to form an external shock in the ISM and sweep up all the surrounding medium. Such a complete-sweeping assumption is commonly adopted in many studies to estimate the long-lasting radio emission from kilonova events (Metzger & Bower 2014; Fong et al. 2016; Horesh et al. 2016; Liu et al. 2020; Bruni et al. 2021; Ricci et al. 2021). However, despite their similar dynamics, kilonovae and supernovae are different in many aspects. The kilonova explosion has a much lesser ejecta mass $\sim 0.01 M_{\odot}$, but with a relatively larger velocity $\sim 0.3c$. This results in a particular diffusion time, $t_d \propto (M/v)^{1/2}$, which is roughly one day, corresponding to the peak time of kilonova emission. Generally speaking, such a diffusion timescale implies that the kilonova emission should be fast-evolving, and the duration should be much shorter than that of supernovae. Besides, supernovae and kilonovae also show differences in the ambient ISM. In case of the progenitor star, core-collapse supernovae usually locate at the H II regions. The continuous UV emission from a bright star can ionize the hydrogen atoms and form the so-called H II bubble. The typical scale for the H II bubble of an OB star is 70 pc. Such a kind of ISM is mostly composed of ionized hydrogens. However, for the mergers of double NSs, they are probably far away from the star-forming region. The ISM densities derived from short-GRB afterglows range from $10^{-4} - 1 \text{cm}^{-3}$ (Metzger & Bower 2014), which are significantly lower than those in H II region. Recently, Agüí Fernández et al. (2023) reported the first chemical study of the ISM in GRB160410A. On the one hand, the X-ray spectrum shows strong Ly α absorption lines, and the column density of $\log(N(\text{HI})/\text{cm}^2) \simeq 21.2$ indicates a damped Ly α host. This is similar to the long GRBs having $\log(N(\text{HI})/\text{cm}^2) > 20.3$ (Tanvir et al. 2019). On the other hand, the spectrum does not show any ionized C_{IV} and Si_{IV} absorption lines. These lines detected in long-GRB afterglows have been assumed to originate from the ionized hot gas in the host galaxy (Ledoux et al. 1998; Wolfe & Prochaska 2000; Heintz et al. 2018). The result implies that this short GRB is still within the galactic H I halo. Therefore, due to the absence of the H II region and the hot diffuse gas, the merger events are likely to be exposed to the neutral H I medium.

If the double NS merger events are indeed within the H I halo, the fast-moving merger ejecta would interact with the ambient ISM, which is mostly composed of neutral hydrogens. In this picture, the free path for the neutral hydrogen atoms should be first dominated by elastic collision.⁷ Years after the explosion, the merger ejecta could become so rarefied that the free path for neutral hydrogen atoms may exceed the scale of the ejecta. As a result, a steady shock is unsustainable, and most of the neutral ISM hydrogens would be neither collided nor swept up by the rarefied ejecta. In this view, the complete-sweeping assumption may be suspicious, especially at late time.

After the nucleosynthesis during the merger explosion, the ejecta is mostly composed of r-process elements, which are heavy metal elements with mass numbers 100-200 (Rosswog et al. 2014; Hotokezaka et al. 2018). After months and years of radioactive decay, these elements mostly convert into iron-peak elements. Based on ⁵⁶Fe,

⁷ Only if the neutral hydrogen atoms are ionized during the shock can the free path be dominated by the plasma effect.

a mass number of $A_r = 150$ is adopted to characterize these elements, for simplicity. The standard value is $m = 1.66 \times 10^{-24} \text{g}$ for one-twelfth of the mass of ^{12}C . Then the ejecta number density for supernovae and kilonovae can be estimated by

$$\begin{aligned} n_{\text{sn}} &= M_{\text{ej}}/mV_{\text{ej}} \\ &= 9.2 \times 10^4 \left(\frac{M_{\text{ej}}}{10M_{\odot}} \right) \left(\frac{v_{\text{ej}}}{10^4 \text{km s}^{-1}} \right)^{-3} \left(\frac{t}{10 \text{year}} \right)^{-3} \text{ cm}^{-3} \end{aligned} \quad (4)$$

and

$$\begin{aligned} n_{\text{kn}} &= M_{\text{ej}}/A_r m V_{\text{ej}} \\ &= 8.4 \times 10^{-4} \left(\frac{M_{\text{ej}}}{0.01M_{\odot}} \right) \left(\frac{v_{\text{ej}}}{0.3c} \right)^{-3} \left(\frac{t}{10 \text{year}} \right)^{-3} \text{ cm}^{-3} \end{aligned} \quad (5)$$

where M_{ej} is the mass, $V_{\text{ej}} = 4\pi R_{\text{ej}}^3/3$ is the volume, $R_{\text{ej}} = v_{\text{ej}}t$ is the radius and v_{ej} is the velocity, respectively. For the density of the supernova ejecta, it is assumed that the ejecta is composed of hydrogens from the stellar envelope of the progenitor. Obviously, the number density of the merger ejecta years later is sufficiently lower than that of the supernova ejecta and even lower than the typical ISM density $\sim 1 \text{cm}^{-3}$. Actually, the merger ejecta is more likely a kind of diffuse cloud that has already left the nebula phase. Combining Equations (3) and (5), one can get the free path for neutral hydrogen atoms:

$$l = 1.2 \times 10^{19} \left(\frac{\sigma}{10^{-16} \text{cm}^2} \right)^{-1} \left(\frac{M_{\text{ej}}}{0.01M_{\odot}} \right)^{-1} \left(\frac{v_{\text{ej}}}{0.3c} \right)^3 \left(\frac{t}{10 \text{year}} \right)^3 \text{ cm} \quad (6)$$

where the cross section for ejecta elements is adopted from solid iron (^{56}Fe). Assuming an average density of $\bar{\rho} = 10 \text{g cm}^{-3}$, the volume for each atom is $\bar{V} = A_r m / \bar{\rho}$. Considering the close packing of metallic atoms, the cross section is then roughly⁸ $\sigma = \bar{V}^{2/3} = 8.5 \times 10^{-16} \text{cm}^2$. This is slightly smaller than the cross section of air molecules. From Equation (6), we can see that the condition $l \ll L$ could be well satisfied at early time with a relatively higher ejecta density. At late time, one can see that the free path $l \propto t^3$ and the radius $R \propto t$. This suggests that the free path will finally exceed the ejecta scale. As a natural consequence, there will be no steady shock at late time, and the ejecta can hardly sweep up the ISM. Therefore, when calculating the shock emission, it is significant to ensure that the ejecta has the ability to sweep up the surrounding medium.

3. THE SWEEPING

Regardless of whether the shock could form, the interaction between the merger ejecta and the ISM first requires that the free path $l \ll L$. Therefore, it is of great significance to determine whether the ambient ISM is ionized or not. Due to the natal kick of the newborn NSs, the binary systems and indeed the merger events more probably locate at the outskirts of the host galaxy, away from the dense H II region. Conservatively, according to Agüí Fernández et al. (2023), it can be inferred

⁸ It is noteworthy that the atomic cross section utilized in our calculation is derived from the ^{56}Fe atom under standard conditions, which may introduce uncertainty in the astrophysical setting.

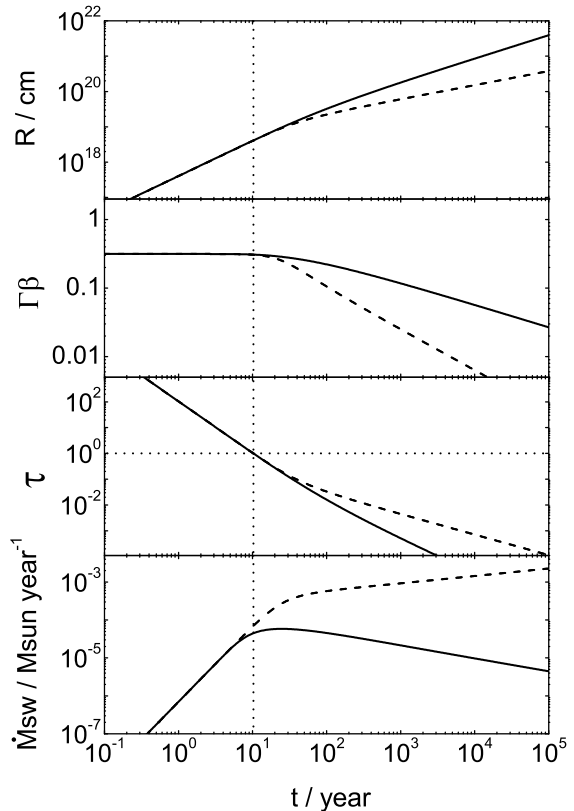


FIG. 1.— The dynamic evolution of the complete-sweeping (dashed lines) and incomplete-sweeping (solid lines) scenarios. The dotted lines show the location where $\tau = 1$. The basic initial parameters are fixed as $M_{\text{ej}} = 0.01M_{\odot}$, $\beta = 0.3$, $n = 10^{-3}$, $p = 2.2$, $\epsilon_e = 0.1$ and $\epsilon_B = 0.1$.

that at least a fraction of short GRBs are still located within the H I halo of their host galaxies. In the subsequent calculations, it is assumed that the merger events are directly within the H I halo, and the ambient ISM is composed of pure neutral hydrogens.⁹ Basically, when the ejecta interacts with the ISM, the neutral ISM hydrogens will be first collided by the ejecta, ionized, and then shocked.¹⁰ Otherwise, the ejecta would continuously move and diffuse in the neutral ISM and no steady shock could form.

In the beginning, the explosion starts at a small volume. The ejecta density is high enough to sweep up all the ambient ISM. Then, the deceleration timescale is

$$\begin{aligned} t_{\text{dec}} &= \frac{(3M_{\text{ej}}/4\pi n)^{1/3}}{v_{\text{ej}}} \\ &= 8.7 \times \left(\frac{n}{0.01 \text{cm}^{-3}} \right)^{-1/3} \left(\frac{M_{\text{ej}}}{0.01M_{\odot}} \right)^{1/3} \left(\frac{v_{\text{ej}}}{0.3c} \right)^{-1} \text{ yr} \end{aligned} \quad (7)$$

where n is the number density of the surrounding medium. To describe the sweeping, one can define a

⁹ The jetted outflow proposed in Margalit & Piran (2020) is not taken into account in this analysis. If the outflow does exist, it can be regarded as an ionized medium.

¹⁰ It is still a collisionless shock in this case, but having first undergone a collisional ionization.

dimensionless parameter with the free path of Equation (6):

$$\tau = \frac{R}{l} = 0.24 \left(\frac{\sigma}{10^{-16} \text{cm}^2} \right) \left(\frac{M_{\text{ej}}}{0.01 M_{\odot}} \right) \left(\frac{v_{\text{ej}}}{0.3c} \right)^{-2} \left(\frac{t}{10 \text{year}} \right)^{-2} \quad (8)$$

When $\tau > 1$, the ejecta can be called thick; otherwise, the ejecta is thin. The ejecta will finally become thin following the explosion. One can define the critical time for such a transition, which is

$$t_{\tau} = 4.8 \left(\frac{\sigma}{10^{-16} \text{cm}^2} \right)^{1/2} \left(\frac{M_{\text{ej}}}{0.01 M_{\odot}} \right)^{1/2} \left(\frac{v_{\text{ej}}}{0.3c} \right)^{-1} \text{year} \quad (9)$$

We can see that the ejecta will become thin several years after the merger. It is sensitive to the parameters when the transition happens. By equating these two timescales, one can get the critical density:

$$n_c = 0.057 \left(\frac{M_{\text{ej}}}{0.01 M_{\odot}} \right)^{-1/2} \left(\frac{\sigma}{10^{-16} \text{cm}^2} \right)^{-3/2}. \quad (10)$$

When the density of the ambient ISM has $n > n_c$, the ejecta would still be thick at the deceleration timescale. That is to say the ejecta would sweep up most of the surrounding medium and be sufficiently decelerated. Otherwise, when $n < n_c$, the ejecta would become thin before the deceleration timescale, which leads to the ejecta being unlikely to sweep up all the medium and keeping its velocity for a much longer timescale.

The previous complete-sweeping assumption is invalid once the ejecta becomes thin, i.e., the free path $l > R$. This means that the expectation of the collision probability for neutral hydrogen atoms is less than 1 during the interaction between the ejecta and the ISM. To estimate the mass of the swept-up medium in the incomplete-sweeping scenario, we use a modified equation,

$$\frac{dM_{\text{sw}}}{dR} = 4\pi R^2 n m_p (1 - e^{-\tau}), \quad (11)$$

where M_{sw} is the total mass of the swept-up medium. The advantage of this equation is that the surrounding medium can be completely swept up when $\tau \gg 1$, but hardly swept up when $\tau \ll 1$. Then, ignoring the energy lost by radiation, the dynamics can be expressed by

$$\frac{d\Gamma}{dR} = - \frac{(\Gamma^2 - 1) 4\pi R^2 n m_p (1 - e^{-\tau})}{M_{\text{ej}} + 2\Gamma M_{\text{sw}}}, \quad (12)$$

together with

$$\frac{dR}{dt} = \frac{\beta c}{1 - \beta}, \quad (13)$$

where Γ is the Lorentz factor. Note that, the dimensionless parameter $\tau = (R/\Gamma)/(l/\Gamma) = R/l$ is unchanged during the Lorentz transformation. With above equations, the dynamic equations can be solved out once the initial parameters are given.

4. THE EMISSION

At late time, the merger ejecta is too thin to sweep up the ISM. Meanwhile, a global steady external shock

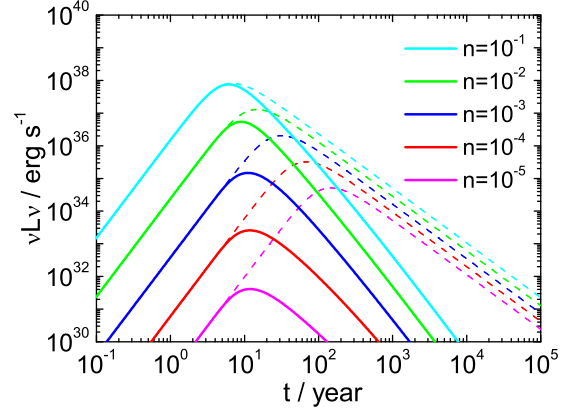


FIG. 2.— The radio (6GHz) lightcurves of complete-sweeping (dashed lines) and incomplete-sweeping (solid lines) scenarios. The basic parameters are the same with Fig.1 but with varied n .

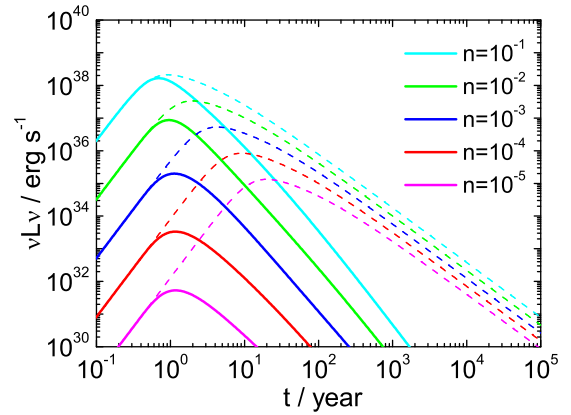


FIG. 3.— The same as Fig.2, but with $M_{\text{ej}} = 0.001 M_{\odot}$ and $\beta = 0.6$.

is unfavored. However, the local shock may exist somewhere, since the ejecta has a density profile or fluctuation. Therefore, the radiation calculation in Nakar & Piran (2011) and Metzger & Bower (2014) is still adopted here, but with a little adjustment. The shocked electrons lose their energy by synchrotron radiation. The flux and the luminosity to the distant observer are

$$F_{\nu} = \frac{(1+z) N_e m_e c^2 \sigma_{\text{T}} \Gamma \beta_{\text{m}}^2 B'}{4\pi D_L^2 3e} \left(\frac{\nu_{\text{obs}}}{\nu_{\text{m}}} \right)^{-(p-1)/2} \quad (14)$$

and

$$L_{\nu} = F_{\nu} 4\pi D_L^2, \quad (15)$$

where the typical synchrotron frequency of electrons is $\nu_{\text{m}} = 3\Gamma \gamma_{\text{m}}^2 \beta_{\text{m}}^2 e B' / 4\pi m_e c$, the minimum electron Lorentz factor is $\gamma_{\text{m}} = ((p-2)m_p / (p-1)m_e) \epsilon_e (\Gamma-1) + 1$ (Liu et al. 2020), and $\nu_{\text{obs}} > \nu_{\text{m}}$, ν_a is adopted in most realistic scenarios, following Nakar & Piran (2011). The parameters $p = 2.2$ and $\epsilon_e = 0.1$ are adopted in this paper. The local magnetic field strength in the shock frame could be estimated by

$$B' = \sqrt{8\pi \tilde{\epsilon}_{\text{B}} (4\Gamma + 3) (\Gamma - 1) \tilde{n} m_p c^2}, \quad (16)$$

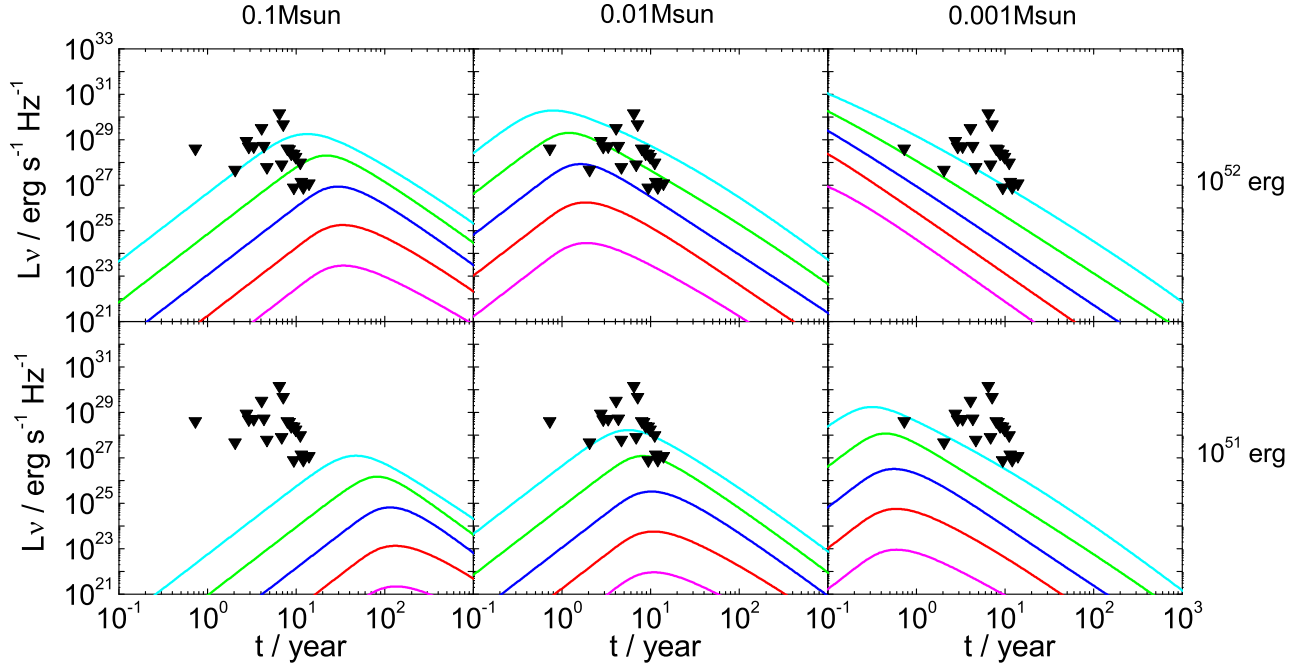


FIG. 4.— The radio lightcurves with different ejecta mass and explosion energy and the comparison with observation. The upper limit data is from Ricci et al. (2021).

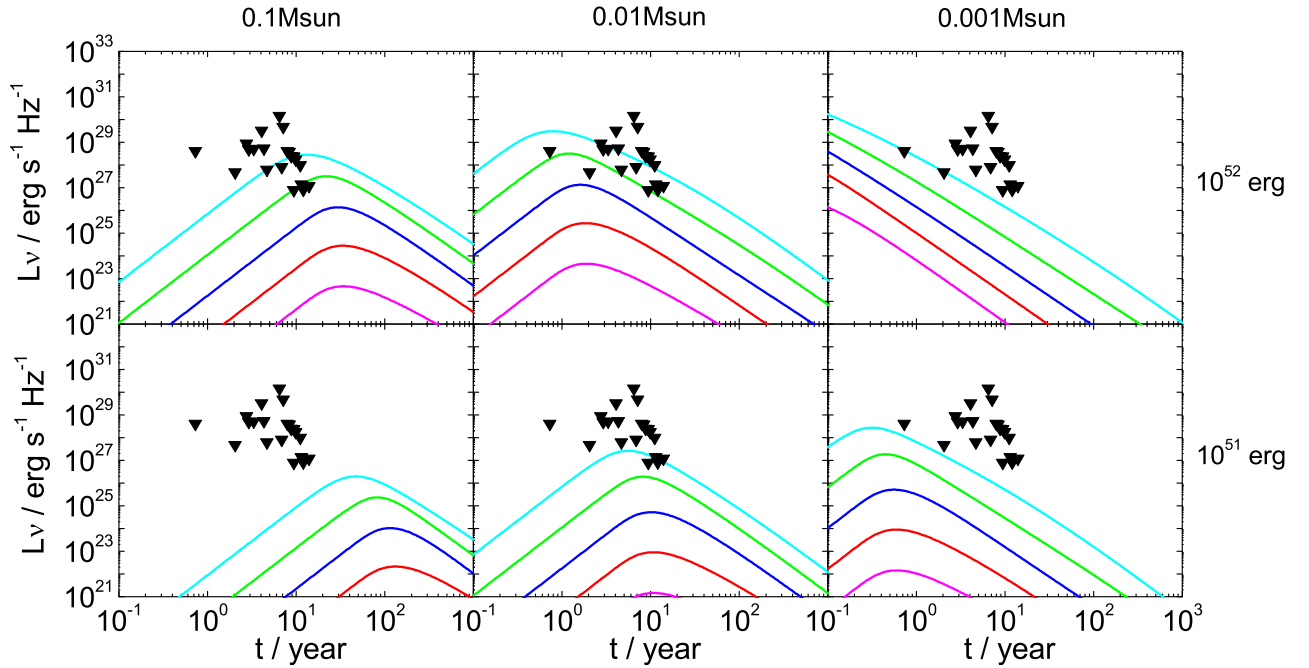


FIG. 5.— The same as Fig.3 but with $\epsilon_B = 0.01$.

where the effective medium density $\tilde{n} = (1 - e^{-\tau})n$. Considering that the shock can not keep steady once $\tau \leq 1$, the shock-induced magnetic energy would decay following the decrease of τ . Here, a similar expression, $\tilde{\epsilon}_B = (1 - e^{-\tau})\epsilon_B$, is adopted to characterize the magnetic energy fraction.

As shown in Fig.1, using typical ejecta parameters, we plot the dynamics of the ejecta in both the complete-sweeping scenario and the incomplete-sweeping scenario.

The outcomes show much difference at late time. In the complete-sweeping scenario (dashed lines), the sweeping rate increases endlessly, even though the ejecta has been sufficiently decelerated. But in the incomplete-sweeping scenario (solid lines), the ejecta reaches $\tau = 1$ before deceleration. After that, when $\tau < 1$, the ejecta becomes thin and the sweeping rate begins to drop. On the one hand, the incomplete sweeping leads to a lower sweeping rate; on the other hand, the ejecta could keep its veloc-

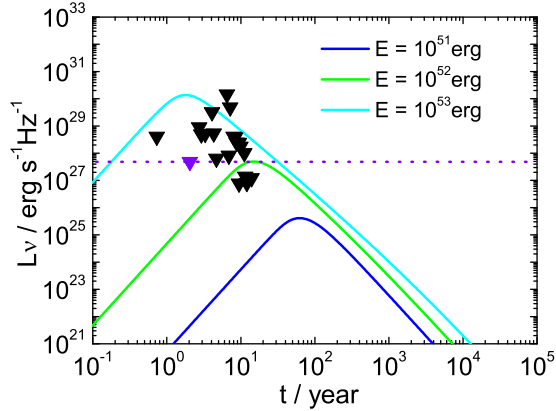


FIG. 6.— Constraints on the kinetic energy of the merger ejecta of GW170817. The ejecta mass and medium density are fixed as $m_{\text{ej}} = 0.06 M_{\odot}$ and $n = 2 \times 10^{-3}$. The limit from GW170817 is marked in violet. The limits from other GRB samples are shown in black for comparison.

ity for a much longer timescale, as mentioned above. As a natural consequence, the energy converted into radiation is decreased. Figure 2 shows the light curves for both scenarios with different ISM densities. It is independent of the medium density when the transition between $l < R$ and $l > R$ happens. The light curves begin to drop at the transition. Therefore, the peak luminosity in the incomplete-sweeping scenario should be at the transition time, $t_{\text{peak}} \simeq t_{\tau}$ ($\tau = 1$), once the precondition $n < n_c$ is satisfied. We can see that for a higher medium density, the difference of the peak luminosity in the complete-sweeping and incomplete-sweeping scenarios is not clear. But for a lower density, the peak luminosity in the incomplete-sweeping scenario is much lower than that in the complete-sweeping scenario. For a better understanding, we plot Figure 3, using various ejecta parameters for comparison. In simple terms, the lesser the ejecta mass and the lower the ISM density, much more different peak luminosities will show in these two scenarios. This is actually determined by Equation (10). It is more sensitive to the parameter n than M_{ej} . However, from Equation (9), the ejecta mass and velocity jointly determine the transition timescale, which takes responsibility for the peak luminosity.

The ejecta cannot sweep up enough medium after the phase transition, and the condition $l \gg R$ for a steady shock is broken. Therefore, the late-time radio emission could be much lower than the estimates in previous studies. Strictly speaking, Equation (14) is inapplicable when the shock is broken. For simplicity, we still calculate the light curves using this equation, in case of what we are concerned about is only the peaks of the light curve. Furthermore, we plot the radio light curves using different initial parameters and then take a comparison with the observation. As shown in Figure 4, for an energetic explosion (e.g., $E_k = 10^{52}$ erg) with a relatively higher ISM density, the light curves may still exceed the upper limit from observations. This is consistent with previous works (Metzger & Bower 2014; Fong et al. 2016; Liu et al. 2020). However, under a relatively lower ISM density, our calculation shows that the light curves are obviously below the upper limit. If the explosion is not power-

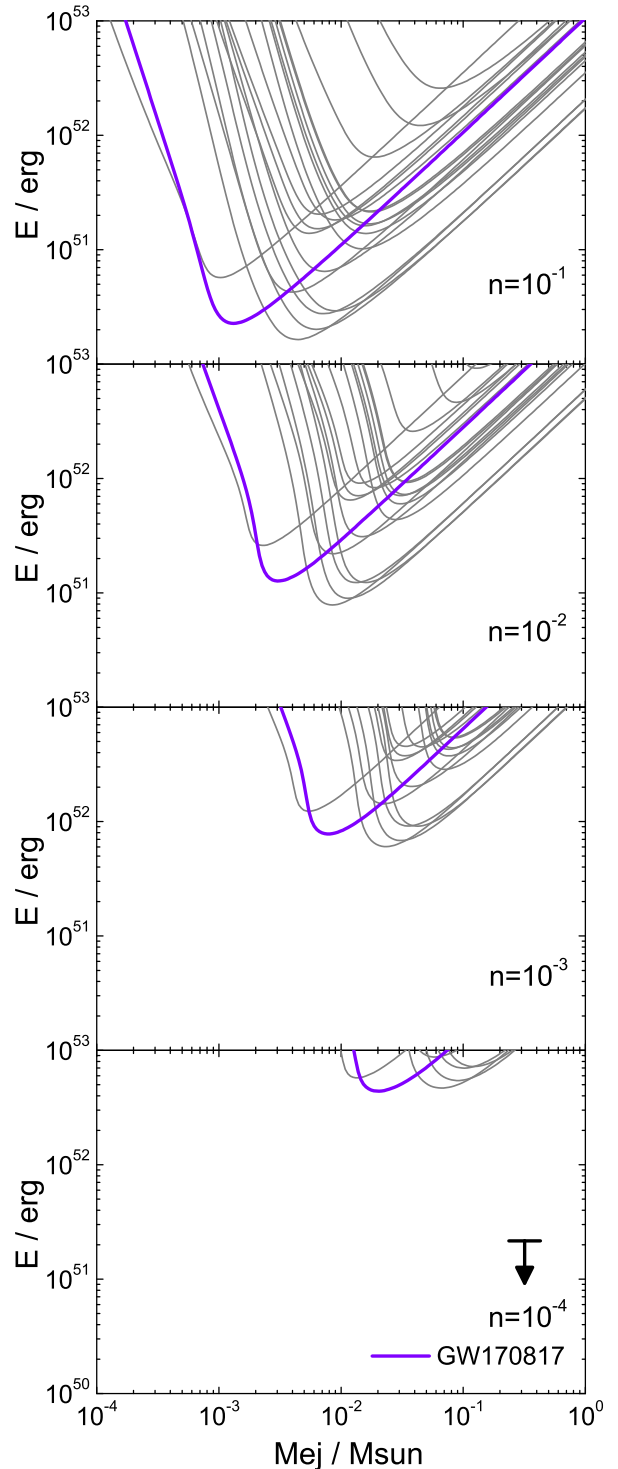


FIG. 7.— Upper limit lines of the constraints on the ejecta mass and kinetic energy from 21 SGRB samples. The violet lines are from the limit of the GW170817 event.

ful enough (e.g., $E_k = 10^{51}$ erg), our results are in accord with the observation: the shock emission is weak and the radio signals can hardly be detected. Furthermore, our calculation pays less attention to the specific radiation

mechanism. According to short-GRB afterglows, a relatively small value of ϵ_B may be favored. It would make the radio signal more undetectable, as shown in Figure 5 (see the detailed discussion in Liu et al. 2020).

5. THE CONSTRAINTS

As the first detection of GW signals from double NS mergers, the GW170817 event gives a chance to investigate the late-time radio emission. First, from the multi-band afterglow of GRB170817A, the ISM density is limited as $n = 2.5_{-1.9}^{+4.1} \times 10^{-3} \text{ cm}^{-3}$ (Hajela et al. 2019). Second, if the associated kilonova (AT2017gfo) is powered by the radioactive decay of r-process elements, the total mass of the merger ejecta is estimated to be roughly $0.06 M_\odot$ (Smartt et al. 2017; Tanaka et al. 2017; Tanvir et al. 2017; Villar et al. 2017). Adopting these two parameters, Figure 6 is plotted to limit the kinetic energy of the merger ejecta. It clearly shows that the late-time radio signal can hardly be detected with either a total energy of 10^{52} erg nor 10^{51} erg . In another case, the required ejecta mass could be much less than $0.06 M_\odot$ if AT2017gfo is powered by an NS or magnetar (Ai et al. 2018; Li et al. 2018; Yu et al. 2018). Therefore, we plot more general constraints on the ejecta mass and kinetic energy in Figure 7. For completeness, all 21 samples from Ricci et al. (2021) are included. The observational limits are converted into upper-limit lines in this plot. One can see that it provides various constraints on the ejecta mass and kinetic energy, depending on the medium density. Each of the lines clearly shows a decline and rise in the energy–Cmass plot. The rise on the right side of the lines corresponds to the complete-sweeping scenario and is consistent with the results in Ricci et al. (2021). For the decline on the left, it corresponds to the incomplete-sweeping scenario. The watershed of the decline and rise is actually determined by Equation (9), where the deceleration timescale and transition timescale get a balance. From Figure 7, an energetic explosion (e.g., $E_k = 10^{52} \text{ erg}$) is definitely allowed in a broad parameter space, especially with low medium densities.

6. CONCLUSION AND DISCUSSION

Observing long-lasting radio emissions from merger events helps us to understand the evolution of the merger

ejecta. The radio emission should be much brighter if the post-merger remnant is an NS instead of a BH. However, based on the reasonable neutral ISM assumption, our results show that the merger ejecta would be too rarefied to sweep up the ISM several years after the explosion. Instead of sweeping, the merger ejecta would eventually diffuse in the ISM, losing its energy over a much longer timescale through atomic collisions or scattering. As a result, the radio signal is too weak to be detected under typical conditions. Even with an NS remnant, it is still hard to catch the radio signal if the density of the ISM is not high enough. Therefore, it is not easy to rule out an NS (or magnetar) remnant with the current observations.

It is usually considered that the merger remnant is rotating near the Kepler period because of its significant orbital angular momentum. With some possible mechanisms, such as magnetic-field-induced ellipticities (Bonazzola & Gourgoulhon 1996; Palomba 2001; Cutler 2002) and various instability modes (Lai & Shapiro 1995; Andersson 1998; Lindblom et al. 1998; Corsi & Mészáros 2009; Dall’osso et al. 2015), the GW radiation becomes significant for such a rapidly rotating NS. Based on short GRBs, Gao et al. (2016) demonstrate that the rotation energy of the merger remnant is probably lost in the GW channel. Lü et al. (2020) find a short-GRB sample as evidence for the GW-dominated afterglow emission. Therefore, it is most likely that only a fraction of the energy could be reflected in the X-ray plateau and kilonova emission, which is only on the order of 10^{51} erg (Rowlinson et al. 2013; Lü et al. 2015; Gao et al. 2016; Yu et al. 2018; Li et al. 2018). With such a total energy, the long-lasting radio signal is hard to detect. Anyhow, the first detection of a post-merger GW signal is still expected, once the advanced LIGO and Virgo reach their designed sensitivity (Abbott et al. 2017c, 2019; Caudill et al. 2021). At that time, the GW observation could help us identify the merger remnant.

This work is supported by the National Natural Science Foundation of China (grant No. 12021003, 11833003, 12303044), National Key R&D Program of China (2021YFA0718500), and the National SKA Program of China (2020SKA0120300, 2022SKA0130100).

REFERENCES

- Abbott, B. P., Abbott, R., Abbott, T. D., et al. 2017a, *Phys. Rev. Lett.*, 119, 161101
- Abbott, B. P., Abbott, R., Abbott, T. D., et al. 2017b, *ApJ*, 851, L16
- Abbott, B. P., Abbott, R., Abbott, T. D., et al. 2017c, *ApJ*, 848, L13
- Abbott, B. P., Abbott, R., Abbott, T. D., et al. 2019, *ApJ*, 875, 160
- Agüí Fernández, J. F., Thöne, C. C., Kann, D. A., et al. 2023, *MNRAS*, 520, 613
- Ai, S., Gao, H., Dai, Z.-G., et al. 2018, *ApJ*, 860, 57
- Ai, S., Gao, H., & Zhang, B. 2020, *ApJ*, 893, 146
- Ai, S., Zhang, B., & Zhu, Z. 2022, *MNRAS*, 516, 2614
- Andersson, N. 1998, *ApJ*, 502, 708
- Bonazzola, S. & Gourgoulhon, E. 1996, *A&A*, 312, 675
- Bruni, G., O’Connor, B., Matsumoto, T., et al. 2021, *MNRAS*, 505, L41
- Caudill, S., Kandhasamy, S., Lazzaro, C., et al. 2021, *Modern Physics Letters A*, 36, 2130022-458
- Corsi, A. & Mészáros, P. 2009, *ApJ*, 702, 1171
- Cowperthwaite, P. S., Berger, E., Villar, V. A., et al. 2017, *ApJ*, 848, L17
- Cutler, C. 2002, *Phys. Rev. D*, 66, 084025
- Dai, Z. G. & Lu, T. 1998a, *A&A*, 333, L87
- Dai, Z. G. & Lu, T. 1998b, *Phys. Rev. Lett.*, 81, 4301
- Dall’Osso, S., Giacomazzo, B., Perna, R., et al. 2015, *ApJ*, 798, 25
- Falcone, A. D., Morris, D., Racusin, J., et al. 2007, *ApJ*, 671, 1921
- Fong, W., Metzger, B. D., Berger, E., et al. 2016, *ApJ*, 831, 141
- Gao, H., Ding, X., Wu, X.-F., et al. 2013, *ApJ*, 771, 86
- Gao, H., Ding, X., Wu, X.-F., et al. 2015, *ApJ*, 807, 163
- Gao, H., Zhang, B., & Lü, H.-J. 2016, *Phys. Rev. D*, 93, 044065
- Gao, H., Zhang, B., Lü, H.-J., et al. 2017, *ApJ*, 837, 50
- Hajela, A., Margutti, R., Alexander, K. D., et al. 2019, *ApJ*, 886, L17
- Heintz, K. E., Watson, D., Jakobsson, P., et al. 2018, *MNRAS*, 479, 3456
- Horesh, A., Hotokezaka, K., Piran, T., et al. 2016, *ApJ*, 819, L22
- Hotokezaka, K., Beniamini, P., & Piran, T. 2018, *International Journal of Modern Physics D*, 27, 1842005
- Klose, S., Nicuesa Guelbenzu, A. M., Michalowski, M. J., et al. 2019, *ApJ*, 887, 206
- Lai, D. & Shapiro, S. L. 1995, *ApJ*, 442, 259
- Ledoux, C., Petitjean, P., Bergeron, J., et al. 1998, *A&A*, 337, 51
- Li, S.-Z., Liu, L.-D., Yu, Y.-W., et al. 2018, *ApJ*, 861, L12
- Lindblom, L., Owen, B. J., & Morsink, S. M. 1998, *Phys. Rev. Lett.*, 80, 4843

- Liu, L.-D., Gao, H., & Zhang, B. 2020, *ApJ*, 890, 102
- Lü, H.-J., Zhang, B., Lei, W.-H., et al. 2015, *ApJ*, 805, 89
- Lü, H.-J., Yuan, Y., Lan, L., et al. 2020, *ApJ*, 898, L6
- Margalit, B. & Metzger, B. D. 2017, *ApJ*, 850, L19
- Margalit, B. & Piran, T. 2020, *MNRAS*, 495, 4981
- Metzger, B. D., Berger, E., & Margalit, B. 2017, *ApJ*, 841, 14
- Metzger, B. D., Giannios, D., Thompson, T. A., et al. 2011, *MNRAS*, 413, 2031
- Metzger, B. D. & Piro, A. L. 2014, *MNRAS*, 439, 3916
- Metzger, B. D. & Bower, G. C. 2014, *MNRAS*, 437, 1821
- Nakar, E. & Piran, T. 2011, *Nature*, 478, 82
- Nicholl, M., Berger, E., Kasen, D., et al. 2017, *ApJ*, 848, L18
- Palomba, C. 2001, *A&A*, 367, 525
- Pian, E., D'Avanzo, P., Benetti, S., et al. 2017, *Nature*, 551, 67
- Radice, D., Perego, A., Zappa, F., et al. 2018, *ApJ*, 852, L29
- Rezzolla, L., Most, E. R., & Weih, L. R. 2018, *ApJ*, 852, L25
- Ricci, R., Troja, E., Bruni, G., et al. 2021, *MNRAS*, 500, 1708
- Rosswog, S., Korobkin, O., Arcones, A., et al. 2014, *MNRAS*, 439, 744
- Rowlinson, A., O'Brien, P. T., Metzger, B. D., et al. 2013, *MNRAS*, 430, 1061
- Sarin, N. & Lasky, P. D. 2021, *General Relativity and Gravitation*, 53, 59
- Sarin, N., Omand, C. M. B., Margalit, B., et al. 2022, *MNRAS*, 516, 4949
- Schroeder, G., Margalit, B., Fong, W.-fai., et al. 2020, *ApJ*, 902, 82
- Shibata, M., Zhou, E., Kiuchi, K., et al. 2019, *Phys. Rev. D*, 100, 023015
- Shibata, M., Fujibayashi, S., Hotokezaka, K., et al. 2017, *Phys. Rev. D*, 96, 123012
- Smartt, S. J., Chen, T.-W., Jerkstrand, A., et al. 2017, *Nature*, 551, 75
- Tanaka, M., Utsumi, Y., Mazzali, P. A., et al. 2017, *PASJ*, 69, 102
- Tanvir, N. R., Levan, A. J., González-Fernández, C., et al. 2017, *ApJ*, 848, L27
- Tanvir, N. R., Fynbo, J. P. U., de Ugarte Postigo, A., et al. 2019, *MNRAS*, 483, 5380
- Troja, E., Piro, L., van Eerten, H., et al. 2017, *Nature*, 551, 71
- Vaughan, S., Goad, M. R., Beardmore, A. P., et al. 2006, *ApJ*, 638, 920
- Villar, V. A., Guillochon, J., Berger, E., et al. 2017, *ApJ*, 851, L21
- Wolfe, A. M. & Prochaska, J. X. 2000, *ApJ*, 545, 591
- Yu, Y.-W., Li, S.-Z., & Dai, Z.-G. 2015, *ApJ*, 806, L6
- Yu, Y.-W., Liu, L.-D., & Dai, Z.-G. 2018, *ApJ*, 861, 114
- Yu, Y.-W., Zhang, B., & Gao, H. 2013, *ApJ*, 776, L40
- Zhang, B. & Mészáros, P. 2001, *ApJ*, 552, L35